Dalton Transactions

Accepted Manuscript

ROYAL SOCIETY OF CHEMISTRY

www.rsc.org/dalton

Core-level photoemission spectra of $Mo_{0.3}Cu_{0.7}Sr_2ErCu_2O_y$, a superconducting perovskite derivative. Unconventional structure/property relations

Sourav Marik[a, b], Christine Labrugere[b], O.Toulemonde[b], Emilio Morán[a], M. A. Alario-Franco[a,*]

[a]Dpto. Química Inorgánica, Facultad de CC.Químicas, Universidad Complutense de Madrid, 28040-Madrid (Spain)
[b]CNRS, Université de Bordeaux, ICMCB, 87 avenue du Dr. A. Schweitzer, Pessac, F-33608, France
*E mail: maaf@quim.ucm.es

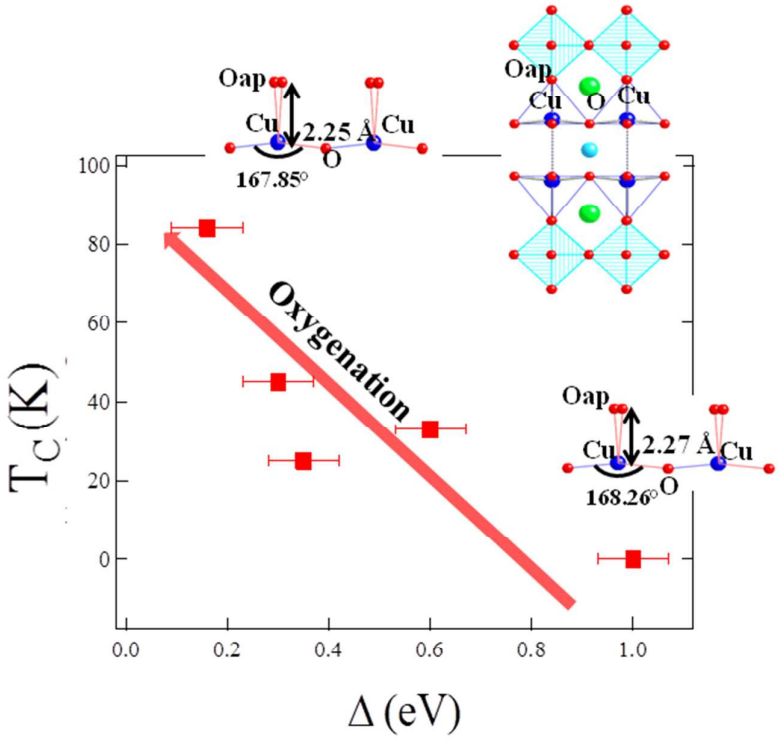

Graphical Abstract: The correlation between the critical temperature, Tc, and the apical oxygen distance, the buckling angle and the charge transfer energy (Δ) along the oxidation, in the family of materials: $Mo_{0.3}Cu_{0.7}Sr_2ErCu_2O_y$

Abstract

Detailed studies of the electronic states for $Mo_{0.3}Cu_{0.7}Sr_2ErCu_2O_y$ samples with different oxygen contents are presented here. The influence of oxygenation in the electronic states for the $Mo_{0.3}Cu_{0.7}Sr_2ErCu_2O_y$ system from a semiconducting to a superconducting state has been investigated by means of X-ray photoelectron spectroscopy (XPS). The XPS studies show that Mo is in a mixed Mo^V and Mo^{VI} oxidation state and Mo^V is predominant over the Mo^{VI} in the as-prepared (AP) sample. Yet annealing under an oxygen atmosphere enhances the Mo^{VI} state. At the same time, a reduction in the copper species is observed. In the Cu 2p spectra, a larger energy separation between the satellite and main peaks (E_S-E_M) and a lower intensity ratio (I_S/I_M) are found to correlate with higher values of the superconducting transition temperature (T_C). Analysis of these spectra within the Configuration Interaction (CI) model suggests that higher values of T_C are related to lower values of the O 2p–Cu 3d charge transfer energy. The change in the Sr 3d and O 1s core level spectra correlates with the oxygen insertion in the $(Mo/Cu)O_{1+\delta}$ chain site, after oxygenation. The hole concentration (P_h) in the copper plane has been obtained using the room temperature thermoelectric power (TEP) value; this shows an increasing tendency in parallel with increasing T_C, after oxygenation. From these experimental results, one observes that T_C *increases* with *decreasing* charge transfer energy. This is, indeed, opposite to accepted views and occurs in parallel with the *shortening* of the apical Copper-Oxygen distance (Cu2–O2) and the *increasing* of the CuO_2 plane buckling angle.

1. Introduction

The Perovskite structure, the most abundant structure in the Earth's mantle, of which about 93% is believed to be the orthorhombic $(Mg,Fe)SiO_3$ [1], appropriately called Bridgmanite [2], is also an extremely important structure on the Earth's surface, given its great relevance to science and technology. Concerning its relevance, and this thematic issue of the Dalton Transactions is an obvious proof of it, one only has to recall the considerable number of materials, and material types, that partake this –beautifully simple, structurally flexible and compositionally adaptable- chemical species, and the almost unlimited number of useful solids that share, rarely, the aristotype and more often than not, one of its multiple variants [3]. Among Perovskite Materials, the celebrated High Temperature Superconducting Cuprates, given birth by the, apparently modest but, in the end, revolutionary paper on $La_{2-x}Ba_xCuO_4$ and its congeners, by Bednorz and Muller [4] constitute the most significant family of superconductors discovered in the last 28 years [5]; but perovskites also occupy a prominent position in the different variants of multiferroicity, giant magnetoresistance, catalysis and various types of sensors [6], to name but a few.

It is widely accepted that high temperature superconductivity in cuprates [7] arises from doping of a Mott-Hubbard insulator [8]. Understanding metal-insulator transitions of doped Mott-Hubbard insulators is one of the outstanding challenges occupying modern solid state shysics. In particular, in the doped cuprates, there exists a complex interplay between lattice, charge, and spin degrees of freedom. Various phases between the antiferromagnetic charge-transfer insulator and the paramagnetic Fermi-liquid like state have been the subject of discussion. The prominent state of matter in this context is superconductivity.

Materials with the 1212 type-structure [9] ($MA_2RECu_2O_{8-\delta}$ or M – 1212, where M, A and RE are commonly a transition metal element, an alkaline earth metal and a rare earth ion, respectively) have drawn a special interest as they are close to the $YBa_2Cu_3O_y$ [10] structure (variously represented as YBCO, $CuBa_2YCu_2O_y$ ($CuSr_2YCu_2O_y$, YSCO) or Cu-1212) having copper in pyramidal coordination with the ligand oxygen. From the Cu-1212-type structures, Mo-stabilized $CuSr_2RECu_2O_y$ (RE = rare earth elements) single phase compounds can be prepared at ambient pressure until reaching the composition $Mo_{0.3}Cu_{0.7}Sr_2RECu_2O_y$

((Mo,Cu)-1212) [11]. This is, indeed, an exciting system to study superconductivity adjacent to a metal-insulator boundary [11-13]. Previous work on Mo-stabilized $CuSr_2RECu_2O_y$ phases showed that these compounds display a superconducting transition centring around 30 K associated to an oxidation reaction from a semiconducting state, with the exception for the bigger RE = La, Pr and Nd compounds, which are not superconducting [14]. However, the superconducting transition temperatures of $Mo_{0.3}Cu_{0.7}Sr_2RECu_2O_y$ materials can be almost as high as that of YBCO when they are oxygenated under high pressure [13, 15-17].

Interestingly, in these compounds, Mo partially adopts the Mo^V oxidation state, which originates magnetic interactions within the charge reservoir layer [11]. As a result, the as-prepared molybdo-cuprate compounds show interesting physical properties [11-13,18,19]. Previous crystal structure studies [11-13,16, 20-22] show that all the $Mo_{0.3}Cu_{0.7}Sr_2RECu_2O_y$ compounds adopt a tetragonal structure with the *P4/mmm* space group. It is noteworthy that contrary to the two-orbital model of Sakakibara et al [23], which shows that T_C increases with the increasing apical copper-oxygen (Cu2–O2) distance, we have found that, in this system, the apical Cu2–O2 distance decreases after oxygenation with increasing T_C for all the 1212-type $Mo_{0.3}Cu_{0.7}Sr_2RECu_2O_y$ compounds [12,13,16]. Moreover, the structural refinement of the as-prepared (non-superconducting) and oxidized (superconducting) phases for the first four members of the homologous series $(Cu_{0.75}Mo_{0.25})Sr_2(Ce,Y)_SCu_2O_{5+2s+\delta}$ by Chmaissem et al.[16] showed that, besides the 1212 compound, the 1222 and 1232 molybdo-cuprate compounds also show the trend of shortening apical oxygen distances after oxygenation. At the same time, in these compounds [12,13,16], the out-of-plane buckling angle [24] increases with oxygenation in disagreement with the common belief that maximum T_C's are achieved when perfectly flat CuO_2 planes are present, as exemplified by mercury cuprate [25].

High-temperature superconductors have been widely studied with photoemission spectroscopy [26]; X-ray photoelectron spectroscopy (XPS) is a powerful tool for studying the doping of the 3d element in the Cu site and can study the electronic structure of the system. Core-level measurements provide information on the electronic states of the compounds, such as oxidation states and doping-induced chemical potential shifts and, in the case of the highly correlated Cu cations, charge-transfer mechanisms and multiplet splitting. The lack of studies on the electronic structure of this interesting molybdo-cuprate family prompted us to investigate the electronic states of 1212-type molybdo-cuprate materials having different oxygen contents and try to relate them to superconductivity, in particular with T_C.

We present and discuss in this paper, a detailed XPS study, of various $Mo_{0.3}Cu_{0.7}Sr_2ErCu_2O_y$, a superstructure of Perovskite, having different oxygen contents and the influence of that in the materials electronic properties, in particular its critical temperature. The evolution of the physical properties with oxygen doping from semiconducting to superconducting, and its consequences in the electronic states, has been investigated and is discussed.

2. Experimental details

The details of the synthesis procedure have been presented elsewhere [11-13]. The sample compositions, annealing (oxygenation process) conditions, and their naming details are presented in Table 1.

Sample purity was checked by powder X-ray diffraction. The oxygen contents were obtained by refining the neutron powder diffraction (NPD) data [13] and thermogravimetric analysis (TGA, data taken under reducing conditions (5% H_2 + 95% N_2). Samples were heated to 973 K, then isothermally maintained for 15 h and cooled down to room temperature. The oxygen content was calculated considering that the final products were Er_2O_3, SrO, $SrMoO_4$ and Cu as observed from the X-ray diffraction.

Physical property measurements were carried out by means of magnetic susceptibility, resistivity and thermoelectric power measurement (TEP) techniques. The resistivity and TEP measurements were carried out in the absence of an applied magnetic field. Magnetic susceptibility measurements were carried out in a 10 Oe magnetic field. The X-ray photoelectron spectroscopy (XPS) measurements were carried out in a Thermo-VG Scientific ESCALAB 220 iXL spectrometer, equipped with a monochromatic Al *K*α X-ray source (1486.6 eV). The samples were scraped in ultra–high vacuum (UHV; 10^{-9} mbar) at room temperature with a stainless steel blade until strong attenuation of the C ls signal was achieved. The spectra were collected with 20 eV constant pass energy. The collected XPS data are fitted with a combination of Gaussian-Lorentzian line shapes, after correction for the Shirley background, by using the AVANTAGE software from Thermofisher Scientific.

3. Results

3.1. Physical properties, oxygen content and hole concentration

Rietveld refinements of the XRD and NPD (for AP, OA and HPO) data of the samples indicate that all the compounds can be isolated as single phases, crystallizing in a tetragonal

structure with space group P4/mmm. The detailed crystal structure using the combination of XRD, NPD and electron diffraction patterns have been discussed elsewhere [13]. The crystal structure of $Mo_{0.3}Cu_{0.7}Sr_2ErCu_2O_y$ along with the schematic diagram is shown in figure 1.

Magnetic susceptibility and resistivity measurements are shown in the supporting material (Figure 1 in supporting material). The AP sample is non-superconducting; however, an oxygenation process induces superconductivity in the material. The superconducting transition temperatures and calculated oxygen contents using different methods, for all the samples, are compared in Table 1. Figure 2a shows the change of T_C with oxygen contents for five different $Mo_{0.3}Cu_{0.7}Sr_2ErCu_2O_y$ samples. It clearly shows that T_C increases with increasing oxygen content in the structure. The materials oxygenated using high pressure show higher superconducting transition temperatures (T_C = 84 K and 89 K for HPO and HPO_80kbar sample, respectively). The hole concentrations (P_h) were calculated from the 290 K TEP (S (290 K)) data using the universal formula [27].

$$S\ (290\ K) = 372 \exp(-32.4\ P_h) \text{ for } 0.00 < P_h < 0.05,$$

$$S\ (290\ K) = 992 \exp(-38.1\ P_h) \text{ for } 0.05 < P_h < 0.155$$

$$S\ (290\ K) = -139\ P_h + 24.2 \text{ for } P_h > 0.\ 155. \qquad (1)$$

The TEP measurements (Figure 2 in the supporting material) show that the hole concentration increases with increasing oxygen content (Figure 2b), as does the T_C. At the same time, the detailed structural studies [12,13] showed that the variation in the superconducting transition temperature is related to short-range oxygen ordering in the chain copper sites ($(Mo/Cu)O_{1+\delta}$) after oxygenation. This indeed increases the effectiveness in the charge transfer to the superconducting layer (CuO_2), resulting in superconductivity.

3.2. XPS core-level measurements

To get a detailed view of the electronic states and the influence of oxygenation on them, notwithstanding that we used a surface probe technique, we have studied the XPS core level spectra for $Mo_{0.3}Cu_{0.7}Sr_2ErCu_2O_y$ samples with different oxygen contents. However, we were unable to perform XPS measurements (with scraping) on the HPO_80kbar sample due to the small amount of sample able to be prepared at such high pressure. The XPS core level spectra for the other $Mo_{0.3}Cu_{0.7}Sr_2ErCu_2O_y$ samples are as follows:

C 1s core level spectra: Two intense peaks of C 1s core electrons at 285eV and at 289 eV are observed before scraping (Figure 3 in the supporting material). This indicates unambiguously two different states of carbon [28]. The peak at 285 eV corresponds to the normal contamination of the surface by carbon while the second one, at 289 eV, is due to the

formation of carbonates on the surface. The samples were then scraped in vacuum at room temperature with a stainless steel blade. A clean surface can, generally, be obtained after a couple of mild scraping over the surface. The effect of cleaning is evident in the strong attenuation of the C ls signal.

Sr 3d core level spectra: Figure 3a compares the Sr 3d core level spectra for the $Mo_{0.3}Cu_{0.7}Sr_2ErCu_2O_y$ samples. All the samples show a doublet corresponding to the transitions from Sr $3d_{3/2}$ (134 eV) and Sr $3d_{5/2}$ (132.4 eV) separated by 1.6 eV [29]. After oxygenation, they clearly show changes in the core level spectra. The intensity of the Sr $3d_{3/2}$ spectra increases after oxygenation. Eventually, for the HPO sample having the highest oxygen content (y = 7.55) among all our samples studied using XPS, Sr $3d_{3/2}$ shows the most intense peak among all the samples. Also, in the same process, the Sr $3d_{3/2}$ spectra are shifted to the lower energy side, with the oxygenation.

It is worth recalling that the Sr atom (Sr-O) resides between the $(Cu/Mo)O_{1+\delta}$ chain and the CuO_2 plane in the (Mo,Cu)-1212 structure (figure 1). The changes in the Sr 3d core level spectra after oxygenation have two possible explanations.

(I) Any changes, structural or compositional in either the copper chain site ($(Cu/Mo)O_{1+\delta}$) or the copper plane should also be reflected in the SrO layer. It is likely that, due to the presence of the extra oxygen in the copper chain site ($(Cu/Mo)O_{1+\delta}$), the Sr 3d core level spectra will show changes after oxygen annealing.

(II) Another reason, not incompatible with the previous one, attributes the changes in the Sr 3d core level spectra to Sr/Er disorder. In the Bi-1222 ($Bi_2Sr_2CaCu_2O_8$) [29] materials, where Sr/Ca disorder occurs easily, the Sr 3d spectra were deconvoluted in two doublets. The lower binding energy (LBE) doublet represents the Sr atom in the SrO layer between copper chain and CuO_2 plane, and the higher binding energy (HBE) doublet represents the Sr atom in the rare earth (or Ca site for the Bi-1222 material) sandwiched between two CuO_2 layers. Similarly, we have deconvoluted the Sr 3d spectra of all the $Mo_{0.3}Cu_{0.7}Sr_2ErCu_2O_y$ samples with two doublets. Figure 3b shows the deconvoluted spectra, and the fitting parameters are shown in Table 2.

The deconvolution of the Sr 3d core level spectra show that the intensity of the HBE doublet increases with oxygenation. This, in fact, points out to the possibility of intermixing between Sr and Er. However, our structural analysis using the joint RT NPD/RT XRD refinement does not show any indication of Sr/Er intermixing [12-13].

It then appears that the changes in the Sr spectra after oxygenation, are related to the variations in structure and composition produced in the $(Cu/Mo)O_{1+\delta}$ chain layers.

Er 4d core level spectra: The core level Er 4d spectra for all the $Mo_{0.3}Cu_{0.7}Sr_2ErCu_2O_y$ samples are shown in Figure 4. They show a peak at 168.2 eV, which is similar to the binding energy observed in pure erbium oxide [30]. No significant change in the Er 4d spectra has been observed after oxygenation. Moreover, the peak position is found to be the same in all cases. This, indeed, corroborates the absence of Sr/Er intermixing after oxygenation in the present samples.

Mo 3d core level spectra: Figure 5 compares the XPS spectra of the Mo 3d core levels for the different $Mo_{0.3}Cu_{0.7}Sr_2ErCu_2O_y$ samples. All the spectra exhibit a two peak structure, typical of 3d core levels with spin orbit splitting. The Mo $3d_{5/2}$ and $3d_{3/2}$ peaks for the AP sample are at 232.1 eV and 235.2 eV respectively. We can observe both peak broadening and peak shifting for the oxygenated samples compared to the AP ones. The difference between the $3d_{5/2}$ and $3d_{3/2}$ peaks is 3.1 eV for all samples. The intensity ratios of the two components are close to 1.5 in all cases, which is expected from the multiplicity of the spin orbit split feature.

However, to get an idea of the oxidation state of molybdenum and the cause of peak broadening and peak shifting, we have continued the fitting on the Mo 3d core level spectra. A spin-orbit splitting of 3.1 eV [31] and a $3d_{5/2}$:$3d_{3/2}$ intensity ratio of 3:2 have been used for the fitting, after appropriate correction of the background with a single Shirley (Gaussian-step) function. The fitted spectra are provided in the supporting material (Figure 4 in supporting material) and the details of the fitting parameters are shown in Table 3.

The fitting of the XPS spectra of Mo 3d core levels allows us to confirm the large content of Mo^V in the AP sample. Mo^V and Mo^{VI} are identified by the energy shifts of their core levels, assigning the doublet at 232 eV and 235.1 eV ($3d_{5/2}$ and $3d_{3/2}$) to Mo^V and the one at 232.9 eV and 236.0 eV ($3d_{5/2}$ and $3d_{3/2}$) to Mo^{VI}, as proposed before [11]. Annealing under an oxygen atmosphere increases the amount of Mo^{VI}.For the HPO sample having the highest oxygen content (y = 7.55), we have found the highest amount of Mo^{VI} (40%, while in the AP sample Mo^{VI} = 24% and y = 7.34; see Table 3).

Cu 2p core level spectra: The Cu $2p_{3/2}$ spectra for all the samples are shown in Figure 6. The Cu $2p_{3/2}$ spectra for all the samples are typical of Cu^{II} compounds. The main peak near 933 eV is attributed to the well-screened $\underline{2p}^5 3d^{10}\underline{L}$ final states resulting from ligand-to-metal (O $2p \rightarrow$ Cu $3d$) charge transfer, and the satellite at higher binding energy corresponds to a multiplet of $\underline{2p}^5 3d^9 \underline{L}$ states, where an underline denotes a hole and L denotes the oxygen ligand [32-36].

In a simplified description of the Cu $2p_{3/2}$ spectrum, to maximize the energy gain, a

doped hole first extends out as a symmetric coherent superposition of the four O 2p hole states surrounding the Cu^{II} ion and then hybridizes with the central Cu d_{x2-y2} hole to form a Zhang-Rice singlet [36]. The ground state of the neutral CuO_4 cluster integrated in an effective medium in an extended configuration-interaction (CI) model [34,37,38] is a superposition of the $|3d^9>$ and $|3d^{10}\underline{L}>$ electronic states. The interaction is described by the hybridization integral $T = <d^9|H|d^{10}\underline{L}>$ and the metal to ligand (Cu 3d→O 2p) charge transfer energy $\Delta = <d^9|H|d^9> - <d^{10}|H|d^{10}>$ is a measure of the bonding–antibonding separation in the ground state.

However, as shown in Figure 6, one can see a clear shoulder (shown by an arrow) and broadening of the Cu $2p_{3/2}$ main peak at the higher binding energy side for the AP sample, which is a characteristic feature of Cu^{III} [39]. Also, the main peak is shifted towards the lower energy side after oxygenation. We have fitted the Cu $2p_{3/2}$ spectra for all the samples. The fitting parameters, the summary of the fitting and the average oxidation state of copper are shown in Table 4. Quite interestingly, *in parallel to the oxidation of the molybdenum species a reduction of the copper is observed in the XPS spectra of the Cu 2p core levels.* The average oxidation state of Cu goes from 2.19 in the AP sample to 2.09 for the HPO sample.

Beside the peak shift, the satellite peak intensity is found to decrease after oxygenation. The satellite peak to main peak intensity ratios (I_S/I_M, Table 5) and their energy separations (E_S-E_M) are calculated using a single Gaussian fitting in the satellite and main peak, respectively. The I_S/I_M ratio shows the lowest value for the HPO sample, having the highest oxygen content (y = 7.55). According to the Configuration Interaction (CI) model, the change in the ratio between the satellite peak and the main peak intensity (I_S/I_M), is associated with a charge transfer energy (Δ) from the O 2*p* to the Cu 3*d* state [33-35]. This ratio goes in parallel with the charge transfer energy: it decreases when the charge transfer energy decreases. In a simple configuration interaction model, I_S/I_M and E_S-E_M, are related to the parameters Δ, T (hybridization integral), and U (on-site Coulomb interaction between Cu 2p and 3d holes):

$$E_S-E_M = ((\Delta-U)^2 + 4T^2)^{1/2}$$

$$I_S/I_M = \tan^2(\varphi-\theta), \text{ where } \tan(2\theta) = 2T/\Delta \text{ and } \tan(2\varphi) = 2T/(\Delta-U) \qquad (2)$$

The charge transfer energy (Δ) is estimated by considering T = 2.2 eV, and U = 7.8 eV, as described previously [37]. Figure 7 shows the variation of T_C with Δ and I_S/I_M. It shows that Δ decreases with oxygenation in parallel with increasing T_C.

O 1s core level spectra: Figure 8a shows the O 1s spectra for all samples. It is apparent that the O 1s spectra exhibit two broad peaks: a higher intensity one at ~528.7 eV and another (shoulder) at ~530.3 eV with lower intensity. However, both peaks are considerably broader for all the samples, which suggest the presence of overlapping multi-components in the samples. In the present system, the oxygen component is complex, since it includes three different sites: the SrO layers, the CuO_2 planes and the $(Mo/Cu)O_{1+\delta}$ site. The present O 1s emissions correspond to the emission from O ions bonded within three different metal-oxide planes: O ions bonded to Mo/Cu in $(Mo/Cu)O_{1+\delta}$ planes, to Sr in SrO layers and to Cu in CuO_2 plane. We have fitted the O 1s spectrum for the OA sample with three different components, and the fitted data is shown in Figure 8b. From the fitting, we can assign the peak at 528.9 eV to O2p–Cu3d bonding, consistent with the studies of other cuprate superconductors [32], while the peak at about 530.3 eV is assigned to O2p-Mo3d bonding [11]. The peak at 531.3 eV, on the other hand, is due to the O bonding to Sr in the SrO layer.

As shown in Figure 8a, the shoulder at 530.3 eV increases after oxygen annealing. The peaks at 528.9 eV and 530.3 eV correspond to the O ions bonded to the CuO_2 planes and $(Mo/Cu)O_{1+\delta}$, respectively. So the enhancement of the shoulder at ~530.3 eV has a correlation with the extra oxygen ions in the $(Mo/Cu)O_{1+\delta}$ planes after oxygenation. The oxygenation enhances the amount of oxygen in the $(Mo/Cu)O_{1+\delta}$ plane; this elevates the amount of the Mo^{VI} state and increases the number of Mo–O bonds and is reflected in the O 1s line shapes related to the O 2p–Mo 3d bonding. It is noteworthy that we have also observed significant changes in the Sr 3d core-level spectra after the introduction of extra oxygen ions in the $(Mo/Cu)O_{1+\delta}$ plane. This suggests that the change in the Sr 3d core level spectra is correlated with the enhancement of the O 1s spectra at the higher energy side after oxygenation.

4. Discussion

Surface electronic structure: At the beginning of this discussion on the electronic states of the scraped $Mo_{0.3}Cu_{0.7}Sr_2ErCu_2O_y$ samples, we emphasized that, in principle, we can only obtain average information from the surface. On the other hand, due to the scraping in ultrahigh vacuum (UHV; 10^{-9} mbar) at room temperature, depth sensitive information has been obtained which can be used to differentiate between surface and bulk electronic states.

As we have seen, the Er 4d core level spectra do not show significant changes after

oxygenation, as expected. However, the Sr 3d and O 1s core level spectra show a complicated scenario. As discussed earlier, two doublets and the changes in the Sr 3d core level spectra after oxygenation have two possible explanations. Nevertheless, the structural analysis [12,13] using diffraction (NPD and XRD) patterns did not show any indication of intermixing of Sr and Er: In fact, the occupancies of Sr and Er become negative when they are allowed to share their opposite Er and Sr sites. At the same time, the Er 4d core level spectra do not show any significant change. Both of these observations rule out the possibility of the amalgamation of Sr and Er in the structure. Our detailed structural studies [12,13] showed the accumulation of oxygen in the copper chain site ($(Cu/Mo)O_{1+\delta}$) after oxygenation: the amount of extra oxygen in the chain site (δ) changes from 0.34 ($(Cu/Mo)O_{1.34}$ in AP) to 0.55 ($(Cu/Mo)O_{1.55}$ in HPO), after HP oxygenation. As the Sr atom (SrO layer) resides between the $(Cu/Mo)O_{1+\delta}$ chain and CuO_2 plane in the structure, the extra oxygen atoms in the copper chain ($(Cu/Mo)O_{1+\delta}$) do change the local chemical environment of the Sr atom, and this is reflected in the core level spectra of the Sr 3d.

From the fitting of O1s spectrum, we have found that the O 1s emissions correspond to the O ions bonding in the three different metal-oxygen planes. It also shows that the shoulder around 530.3eV corresponds to the O2p–Mo3d bonding that increases after oxygenation. Therefore, our study suggests that the observed changes in the Sr 3d and O 1s spectra are correlated. The extra oxygen after oxygenation increases the average number of oxygen bonds with Sr and Mo, which changes the chemical environment of the Sr atom as is reflected in the core level spectra of the Sr 3d and the O 1s.

Redox Process: Figure 9 shows the relative energy shift of the Mo3d and Cu2p core level spectra with oxygenation. This emphasizes the shift of the Mo3d and Cu2p core level spectra in opposite sides of the energy region; this indicates the simultaneous oxidation of Mo^{V} and reduction of Cu^{III}. Fitting the Mo 3d and Cu 2p core level spectra allows us to propose a very interesting doping mechanism upon oxidation:

$$Mo^{V}_{x}Mo^{VI}_{(0.3-x)} + Cu^{III}_{y}\,Cu^{II}_{(2.7-y)} \leftrightarrow Mo^{V}_{(x-m)}\,Mo^{VI}_{(0.3-x+m)} + Cu^{III}_{(y-n)}\,Cu^{II}_{(2.7-y+n)} \qquad (3)$$

Where $0 \leq (x-m) \leq 0.3$ and $0 \leq (y-n) \leq 2.7$

This apparently contradictory redox mechanism is feasible because copper (III) oxides tend to decompose at moderate temperatures. $KCuO_2$ decomposes [40] in an oxygen atmosphere at 760 K, a tendency that is characteristic of the higher oxidation states of the elements of the first transition series; likewise, $Cr^{VI}O_3$ decomposes below 570 K. However, in the second and third transition metals rows, the higher oxidation states are more stable. In the case of the

oxides of Mo and W, in the same group (VI) as chromium, the highest oxidation state (VI) is the most stable: $Mo^{VI}O_3$ sublimes in air without decomposing at temperatures above 1430 K [41].

As we have copper on two different sites (Cu1 and Cu2), it is not possible to estimate the accurate hole concentration in the CuO_2 plane (nor the oxidation state of copper for each individual site) from the present XPS results. Yet TEP measurements, a bulk property, show the enhancement of the hole concentration with increasing oxygen content. It then appears that the oxidation of Mo^{V} to Mo^{VI}, present only in the (Cu/Mo) chains, produces enough holes so as to compensate for the reduction of Cu^{III} and T_C, increases, a substantial amount, up to 84 K (HPO sample). Also, the sample (HPO_8GPa) oxidized at 80 kbar shows the onset of a superconducting transition temperature at 89 K, the highest ever observed in this family. Although the present oxidation conditions, 50 kbar and 80 kbar at 773 K, are already highly oxidising, the ever-increasing trend in the functionality of T_C with such parameters suggests that even higher T_C values could be obtained under extreme conditions, since we have not attained the overdoped regime.

Charge transfer energy and orbital admixture: As shown in Figure 7, the superconducting transition temperature shows an increasing trend with decreasing I_S/I_M and, consequently, Δ. Studying the $Bi_2Ca_{1-x}RE_xSr_2Cu_2O_{8+s}$ (RE = Rare Earth) series, Rao el. al. [42] showed that the satellite intensity goes through a minimum at around the same composition where the hole concentration and T_C show maxima. But the oxygen contents were assumed to be the same for all compounds in their studies. However, a recent study with YBCO showed that the I_S/I_M ratio (and then the charge transfer energy Δ) *increases* with increasing oxygen content, and this is associated with a hike in T_C [43]. It is worth recalling here that our materials have a structure similar to YBCO, which prompted us to compare our results with those of YBCO. In $Mo_{0.3}Cu_{0.7}Sr_2ErCu_2O_y$ we have observed a *decrease* in both the I_S/I_M ratio and the overall oxidation state of copper after oxygenation (Table 4); this is correlated with the *decrease* in the charge-transfer energy.

Besides the interesting evolution of the electronic states, some remarkable and unconventional structural points have also been observed for the present materials. As indicated above, in all the studied 1212-molybdo-cuprate compounds [12,13,16] a contraction in the apical Cu2–O2 (d_{apical}) bond length is observed after oxygenation (Figure 10a) with increasing T_C. The role of apical oxygen (O2 in the present materials) in high-T_C superconductivity has been suggested to have great importance [44-49]. For instance,

empirically, the presence of the apex oxygen atoms makes the CuO_2 plane easier to dope with holes. The compounds with square coordination have not been doped successfully but those with copper in octahedral coordination have been made over-doped [50]. Also, the study of the effect of pressure on T_C shows that the T*-phase superconductor with pyramidal copper coordination (having oxygen atoms at the apex) has a very large pressure enhancement of T_C. On the other hand, in the T'-phase superconductor where copper is square planar coordinated, the pressure coefficient of T_C is negligibly small [45]. The structural results then clearly indicate that the apical oxygen is indeed playing an important role in assisting charge transfer between the $(Mo/Cu)O_{1+\delta}$ chain and the CuO_2 copper plane in the transformation from semiconducting to superconducting. On the other hand, Sakakibara et al., [51] proposed that shortening the apical O distance (Cu2–O2) increases the admixture of the Cu $3d_{3z2-r2}$ orbital with the in-plane Cu $3d_{x2-y2}$ orbital, and this decreases T_C. In fact, in single-layer cuprates, increasing the apical oxygen distance reduces the charge-transfer energy, which increases the superconducting transition temperature [51, 52]. We can recall that $HgBa_2Ca_2Cu_3O_{8+\delta}$ show the largest T_C having a large apical distance and an almost flat copper plane [25, 51-54]. Therefore, shortening the apical oxygen distance in the oxygenated superconducting (Mo,Cu)−1212 samples could worsen the hole transfer (charge transfer) from the copper chain site. Nevertheless, our TEP measurements show that hole concentration in the CuO_2 plane *increases* after oxygenation in the present materials. Recent theoretical work by Yee et al. [55], in contrast with Sakakibara et al. [51], proposes that the charge transfer energy controls the strength of correlations and therefore tunes the maximum superconducting transition temperature. Starting with the most correlated cuprate, La_2CuO_4, reducing the charge transfer energy enhances T_C. Chmaissem et al. [55] showed that the hole concentration per CuO_2 plane would increase with a displacement of apical O toward the CuO_2 plane after oxygenation. At the same time, moving the apical oxygen towards the copper plane makes the copper plane buckle, increasing electron-electron repulsion; this is supposed to damage the superconducting properties. However, it is worth emphasizing here that structural studies on the present, and related, materials [12,13,16] have shown the enhancement of the buckling in the CuO_2 plane after oxygenation *in parallel* with increasing T_C (figure 10b).

Therefore, in agreement with Yee et al. [55], our experimental results indicate that charge transfer energy is tuning the superconducting transition temperature (T_C) and in the present system, T_C *increases* with *decreasing* charge transfer energy. This is occurring in

parallel with the shortening of the apical O distance (Cu2–O2) and increasing the CuO_2 plane buckling, while the two orbital model [51] predicts the opposite effect.

5. Conclusions

The detailed studies on the electronic states for the $Mo_{0.3}Cu_{0.7}Sr_2ErCu_2O_y$ samples and the influence of oxygenation in the same are presented here. The present results clearly corroborate the all-important role of apical oxygen in the strength of the charge transfer between the charge reservoir layer – $(Mo_{0.3}Cu_{0.7})O_{1+\delta}$ chains – and the CuO_2 superconducting copper planes in the transformation from a semiconducting to a superconducting state; however, this relation does not seem to have a single-type of functionality. The XPS studies on the Mo 3d and Cu 2p core level spectra allow us to propose a very interesting doping mechanism upon oxidation. The changes in the Sr 3d and O 1s core level spectra are related to oxygen insertion in the $(Mo/Cu)O_{1+\delta}$ chain sites. Analysis of the Cu 2p core level spectra within the Configuration Interaction (CI) model suggests that higher values of T_C are related to low values of the O 2p–Cu 3d charge transfer energy, which is contrary to accepted views, occurring in parallel with the *shortening* of the apical copper-oxygen distance (Cu2–O2) and the *increasing* of the CuO_2 plane buckling angle. Under the present oxidizing conditions, T_C values up to 89 K have been obtained. From the observed trend in the relation between T_C and PO_2, one may expect even higher Tc's or, alternatively, a change from the underdoped to the overdoped regime.

Acknowledgements

The authors are indebted to the European Union through the SOPRANO project (Seventh Framework Programme FP7/2007–2013 under Grant Agreement no. 214040) for funding this work and providing a Marie Curie grant to S. Marik. REE (Red eléctrica de España), the Spanish 'Ministerio de Ciencia e Innovacion' and 'Comunidad de Madrid' are also acknowledged for financial support given through projects REE/UCM 2014, MAT2010-19460 and S2009/PPQ-1626, respectively.

References

[1] M. Murakami, Y. Ohishi, N. Hirao and K. Hirose, Nature, 2012, **485**, 90–94.

[2] O. Tschauner, and C. Ma, Bridgmanite, 2014, IMA 2014-017. CNMNC Newsletter No. 21, August 2014, page 798; Mineralogical Magazine, **78**, 797-804.

[3] R. H. Mitchell, in Perovskites: Modern and Ancient, 2003, Almaz.

[4] J. G. Bednorz and K. A. Muller, Z Phys. B-Condensed Matter, 1986, **64**,189-193.

[5] J. P. Attfield, J. Mater. Chem, 2011, **21**, 4756-4764.

[6] R. Coontz, in Science's Top 10 Breakthroughs of 2013, 19 December 2013.

[7] J. G. Bednorz and K. A. Muller, Phys. Rev. B, 1986, **50**, 3458.

[8] M. Imada, A. Fujimori and Y. Tokura, Rev. Mod. Phys., 1998, **70**, 1039.

[9] L. Bauernfeind, W. Widder and H. F. Braun, Physica C, 1995, **254**,151-158.

[10] P. H. Hor, R. L. Meng, Y. Q. Wang, L. Gao, Z. J. Huang, J. Bechtold, K. Forster and C. W. Chu, Phys. Rev. Lett., 1987, **58**, 1891.

[11] S. Marik, E. Moran, C. Labrugere, O. Toulemonde and M. A. Alario-Franco, J. Solid State Chem., 2012, **191**, 40-45.

[12] S. Marik, A. J. Dos Santos-Garcia, E. Morán, O. Toulemonde and M. A. Alario-Franco, Journal of Physics-Condensed Matter 2013, **25**, 165704.

[13] S. Marik, A. J. Dos Santos-Garcia, E. Morán, O. Toulemonde and M. A. Alario-Franco, Superconductor Science and Technology, Accepted.

[14] Q. Xiong, Y. Y. Xue, J. W. Chu, Y. Y. Sun, Y. Q. Wang, P. H. Hor and C. W. Chu, Phys. Rev. B, 1993, **47**, 11337.

[15] V. P. S. Awanaa, A. Gupta, H. Kishan, E. Takayama-Muromachi, T. Watanabe, M. Karppinen, H. Yamauchi, S. K. Malik, W. B. Yelon, V. Ganesan and A. V. Narlikar, Solid State Commun., 2003, **129**, 117-121.

[16] I. Grigoraviciute, H. Yamauchi, M. Karppinen and M. Marezio Phys. Rev. B, 2010, **82**, 104507.

[17] I. Grigoraviciute, M. Karppinen, Chan Ting-Shan, Liu Ru-Shi, Chen Jin-Ming, O. Chmaissem and H. Yamauchi, JACS, 2010, **132**, 838-841.

[18] H. L. Tsay, C. R. Shih, Y. C. Chen, W. H. Lee, T. H. Meen and H. D. Yang, Physica C, 1995, **252**, 79-86.

[19] H. L. Tsay, Y. C. Chen, S. S. Weng, C. F. Chang and H. D. Yang, Phys. Rev. B, 1999-I, **59**, 636-640.

[20] S. F. Hu, R. S. Liu, S. C. Su, D. S. Shy and D. A. Jefferson, J. Solid State Chem., 1994, **112**, 203.

[21] R. L. Harlow, G. H. Kwei, R. Suryanarayanan and M. A. Subramanian, Physica C, 1986, **257**, 125-136.

[22] T. A. William, S. R. Harrison, J. T. Vaughey, L. Liu and A. J. Jacobson, J. Solid State Chem., 1995, **119**, 115-119.

[23] H. Sakakibara, H. Usui, K. Kuroki, R. Arita and H. Aoki, Phys. Rev. Lett., 2010, **105**, 057003.

[24] B. Buchner, M. Breuer, A. Freimuth and A. P. Kampf, Phys. Rev. Lett., 1993, **73**, 1841-1844.

[25] X. Zhang, W. H. Lu and C. K. Ong, Physica C, 1997, **289**, 99-108.

[26] F. U. Hillebrecht, J. Fraxedas, L. Ley, H. J. Trodahl, J, Zaanen, W, Braun, M, Mast, H, Petersen, M, Schaible, L. C. Bourne, P. Pinsukanjana and A. Zettl, Phys. Rev. B, 1989, **39**, 236.

[27] Y. Ando, A. N. Lavrov, S. Komiya, K. Segawa and X. F. Sun, Phys. Rev. Lett., 2001, **87**, 017001-1.

[28] J. F. Moulder, W. F. Stickle, P. E. Sobol, and K. D. Bomben, Handbook of X-Ray photoelectron spectroscopy; Physical Electronics, U.S.A., Inc.: 1995.

[29] M. Khaled, P. Srivastava, B. R. Sekhar, K. B. Garg, S. K. Agarwal, A. V. Nalikar and F. Studer, J. Phys. Chem Solids, 1998, **59**, 777-782.

[30] Y. Uwamino, Y. Ishizuka, H. Yamatera, J. Electron Spectrosc. Relat. Phenom., 1984, **34**, 67.

[31] A. Katrib, V. Logie, M. Peter, P. Wehrer, L. Hilaire and G. Maire, J. Chim. Phys. Phys.-Chim. Biol., 1997, **94**, 1923.

[32] S. Larsson, Chem. Phys. Lett., 1976, **40**, 362.

[33] G. Van der Laan, C. Westra, C. Haas and G. A. Sawatzky, Phys. Rev. B, 1981, **23**, 4369.

[34] F. Parmigiani and L. Sangaletti, J. Electron Spectrosc. Relat. Phenom., 1994, **66**, 223.

[35] R. P. Vasquez, D. L. Novikov, A. J. Freeman and M. P. Siegal, Phys. Rev. B, 1997-I, **55**, 14623.

[36] F. C. Zhang and T. M. Rice, Phys. Rev. B, 1988, **37**, 3759.

[37] J –J. Yeh, L. Lindau, J.-Z. Sun, K. Char, N. Missert, A. Kapitulnik, T. H. Geballe, and M. R. Beasley, Phys. Rev. B, 1990, **42**, 8044.

[38] K. Okada and A. Kotani, J. Phys. Soc. Jpn., 1989, **58**, 2578–2585.

[39] K. Allan, A. Campion, J. Zhou and J. B. Goodenough, Phys. Rev. B, 1990, **41**, 11572.

[40] Giorgio A. Costa and E. Kaiser, Thermochimica Acta, 1995, **20**, 591-598.

[41] N.N. Greenwood and A. Earnshaw, Chemistry of the elements, Pergamon Press, Oxford 1984.

[42] C. N. R. Rao, G. Rao. Ranga, M. K. Rajumon and D. D. Sarma, Phys. Rev. B, 1990, **42**, 1026.

[43] K. Maiti, J. Fink, S. Jong, M. Gorgoi, C. Lin, M. Raichle, V. Hinkov, M. Lambacher, A. Erb and M. Golden, Phys. Rev. B, 2009, **80**, 165132.

[44] E. Kaldis, P. Fischer, W. Hewat, E. A. Hewat, J. Karpinski and S. Rusiecki, Physica C, 1989, **159**, 668.

[45] C. Murayama, N. Mori, S. Yomo, Takagi, S. Uchida and Y. Tokura, Nature, 1989, **339**, 293.

[46] K. A. Muller, Z. Phys. B, 1990, **80**, 193.

[47] H. Matsukawa and H. Fukuyama, J. Phys. Soc. Jpn., 1990, **59**, 1723.

[48] T. Tohyama and S. Maekawa, J. Phys. Soc. Jpn., 1990, **59**, 1760; Physica B, 1990, **165-166**, 1019.

[49] Y. Ohta, T. Tohyama and S. Maekawa, Phys. Rev. B, 1991, **43**, 2968.

[50] J. B. Torrance, A. Bezinge, A. I. Nazzal, T. C. Huang, S. S. P. Parkin, D. T. Keane, S. J. LaPlaca, P. M. Horn and G. A. Held, Phys. Rev. B, 1989, **40**, 8872.

[51] H. Sakakibara, H. Usui, K. Kuroki, R. Arita and H. Aoki, Phys. Rev. Lett., 2012, **85**, 064501.

[52] C. Weber, C. Yee, K. Haule and G. Kotliar, EPL, 2012, **100**, 37001.

[53] O. Chmaissem, Q. Huang, E. V. Antipov, S. N. Putilin, M. Marezio, S. M. Loureiro, J. J. Capponi, J. L. Tholence and A. Santoro, Physica C, 1993, **217**, 265.

[54] C. W. Chu, L. Gao, F. Chen, Z. J. Huang, R. L. Meng and Y. Y. Xue, Nature, 1993, **365**, 323-325.

[55] C. –H. Yee and G. Kotliar, Phys. Rev. B, 2014, **89**, 094517.

[56] O. Chmaissem, J. D. Jorgensen, S. Short, A. Knizhnik, Y. Eckstein and H. Shaked, Nature, 1999, **397**, 45.

Figures:

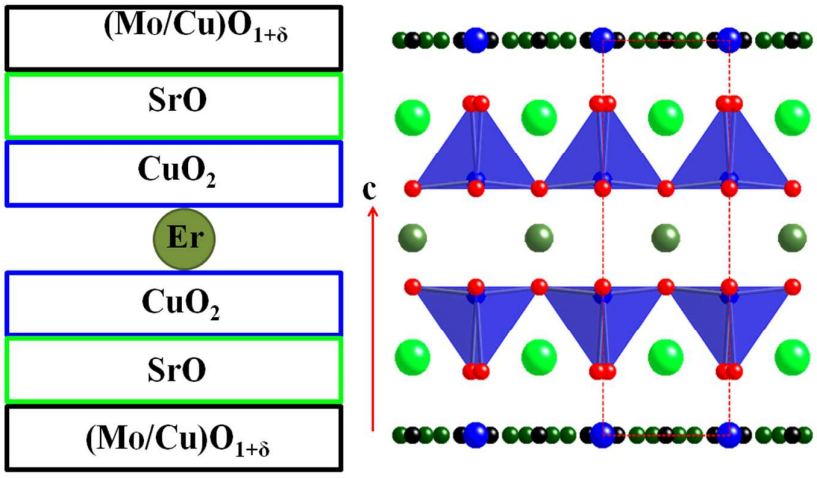

Figure 1. Schematic diagram of the (Mo,Cu)-1212Er structure ($Mo_{0.3}Cu_{0.7}Sr_2ErCu_2O_y$, Tetragonal, *P4/mmm*) along with the crystal structure as suggested by NPD refinement (see ref. 6 and 7). Two different chain oxygen ions are highlighted in black and deep green; other oxygen ions are shown as red spheres. The detailed structural analysis and oxygen positions are described in ref. 6.

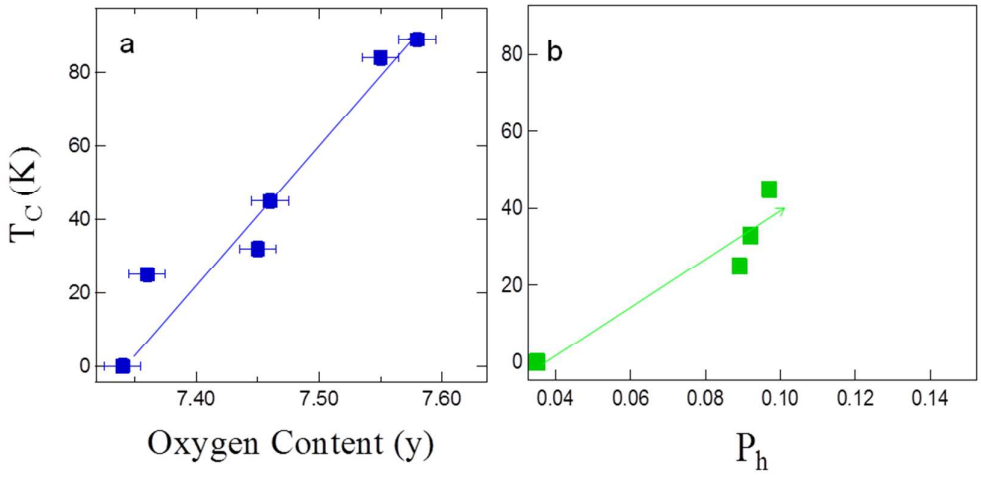

Figure 2. (a) Variation of T_C with oxygen contents for the different $Mo_{0.3}Cu_{0.7}Sr_2ErCu_2O_y$ samples. (b) Variation of T_C with hole concentration (P_h), calculated using 290K TEP data. It shows that the hole concentration increases with increasing oxygen content in the structure, as does the T_C.

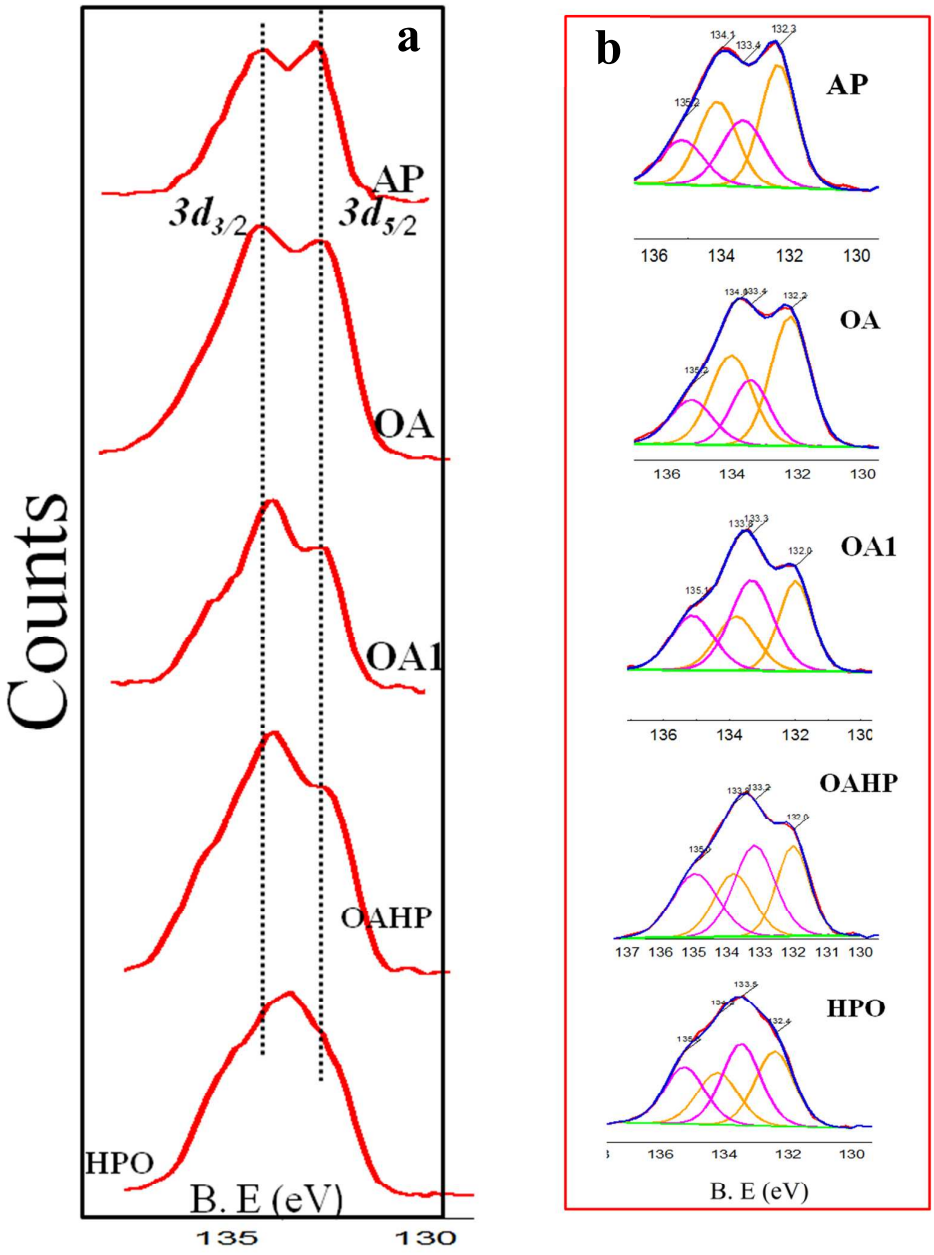

Figure 3. (a) Core level XPS spectra for the Sr 3d energy region for the $Mo_{0.3}Cu_{0.7}Sr_2ErCu_2O_y$ samples. The intensity of the Sr $3d_{3/2}$ spectra increases and shifts towards lower binding energy side after oxygenation. (b) Fitted Core level XPS spectra for the Sr 3d energy region for the same. The spectra have been deconvoluted using two doublets. The lower binding energy (LBE) doublet represents the Sr atom in the SrO layer between copper chain and CuO_2 plane and the higher binding energy (HBE) doublet represents the Sr atom in the rare earth (Er) site, sandwiched between two CuO_2 layers.

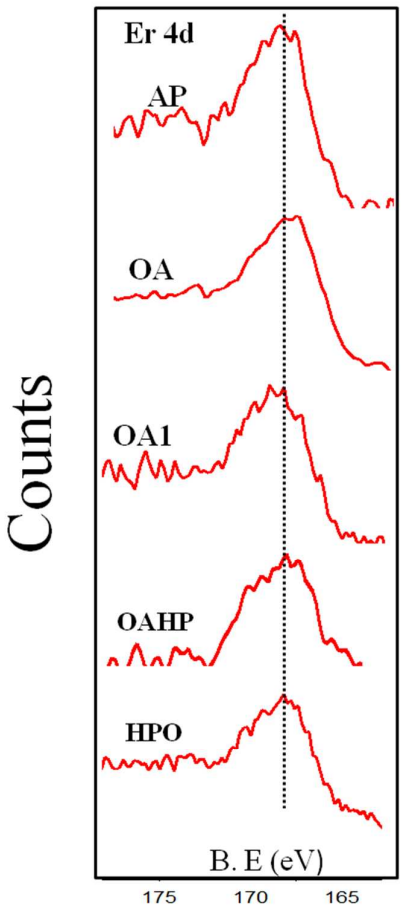

Figure 4. Core level XPS spectra of Er 4d energy region for the $Mo_{0.3}Cu_{0.7}Sr_2ErCu_2O_y$ samples. No significant change in the Er 4d spectra has been observed after oxygenation. The peak position is found to be the same in all cases.

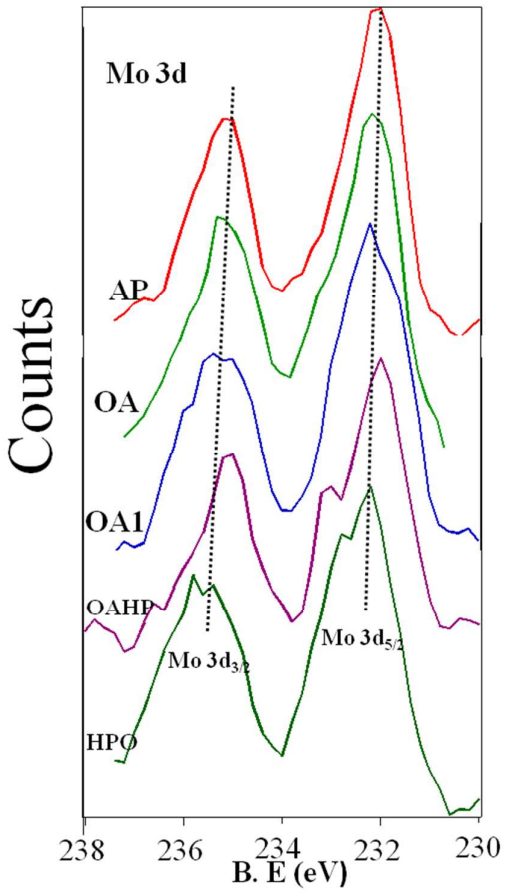

Figure 5. Core level XPS spectra of Mo 3d energy region for the $Mo_{0.3}Cu_{0.7}Sr_2ErCu_2O_y$ samples. Both peak broadening and peak shifting are observed for the oxygenated samples compared to the AP one; this indicates the oxidation of Mo with increasing oxygen content in the structure.

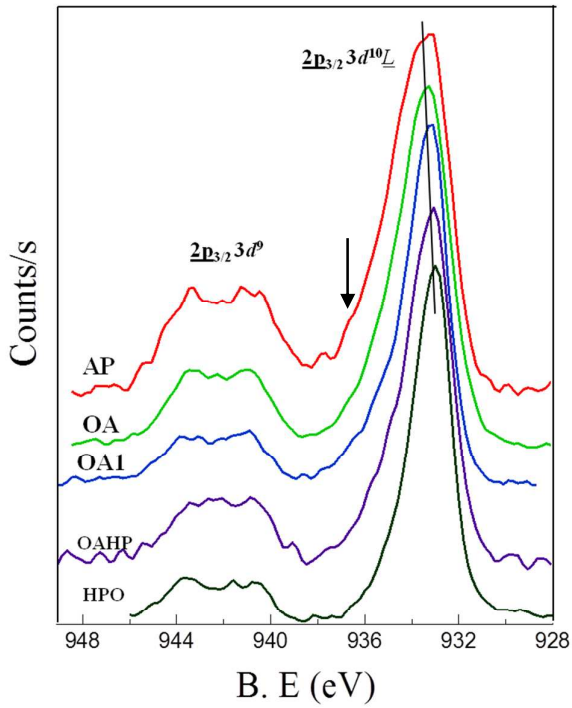

Figure 6. Core level XPS spectra of $Cu2p_{3/2}$ energy region for the $Mo_{0.3}Cu_{0.7}Sr_2ErCu_2O_y$ samples. The Cu^{III} characteristic shoulder is shown by an arrow.

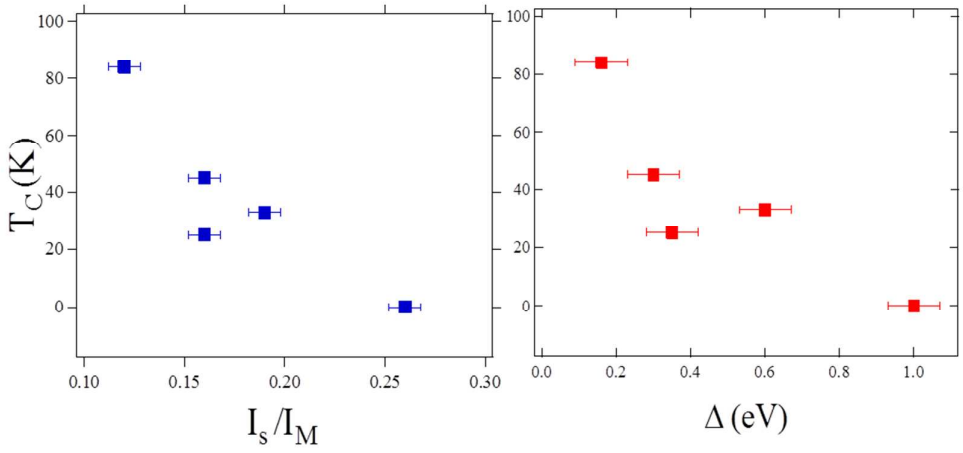

Figure 7. Variation of T_C with (a) I_S/I_M and (b) charge transfer energy (Δ) along the oxidation process. It shows that T_C increases with decreasing Δ.

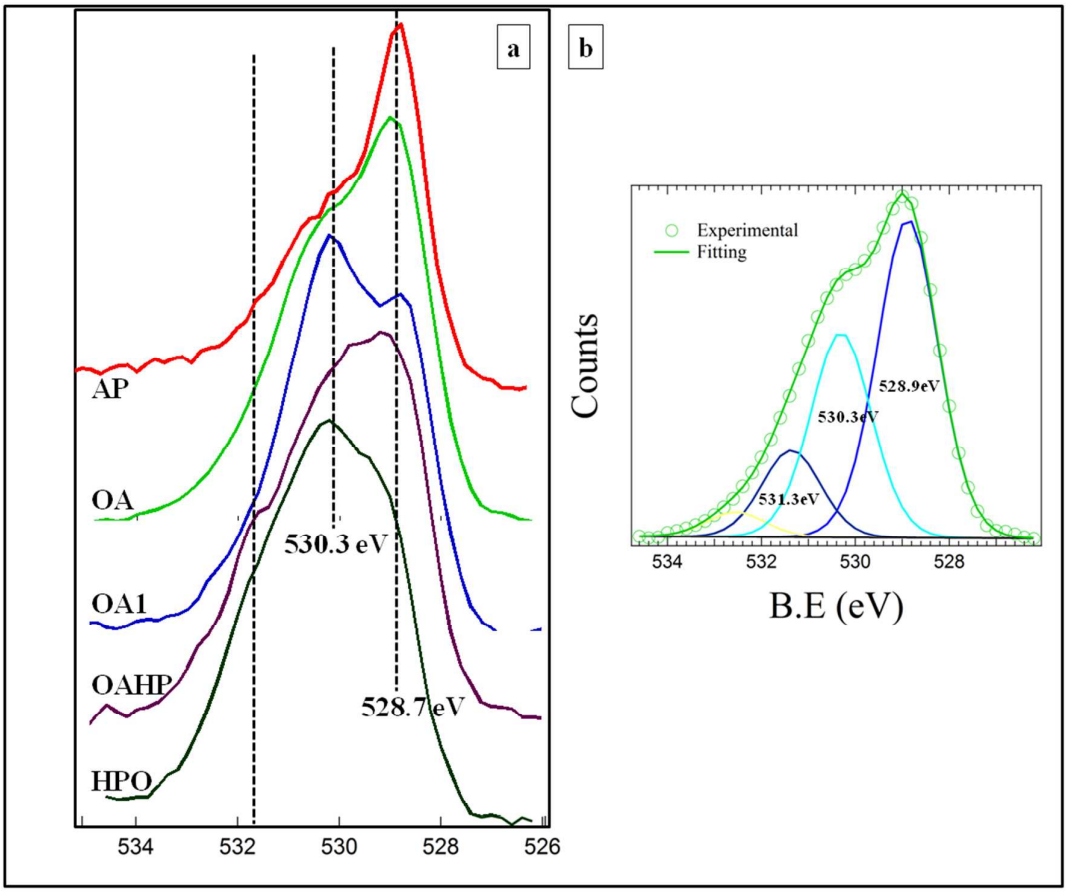

Figure 8. (a) Core level XPS spectra of O1s energy region for the $Mo_{0.3}Cu_{0.7}Sr_2ErCu_2O_y$ samples. (b) Fitted O 1s spectrum for the OA sample. The peak at 528.9 eV is assigned to the O2p-Cu3d bonding, consistent with the studies of other cuprate superconductors[26], while the peak at about 530.3 eV is assigned to O2p-Mo3d bonding. The peak at 531.3eV is due to the O bonding to Sr in the SrO layer.

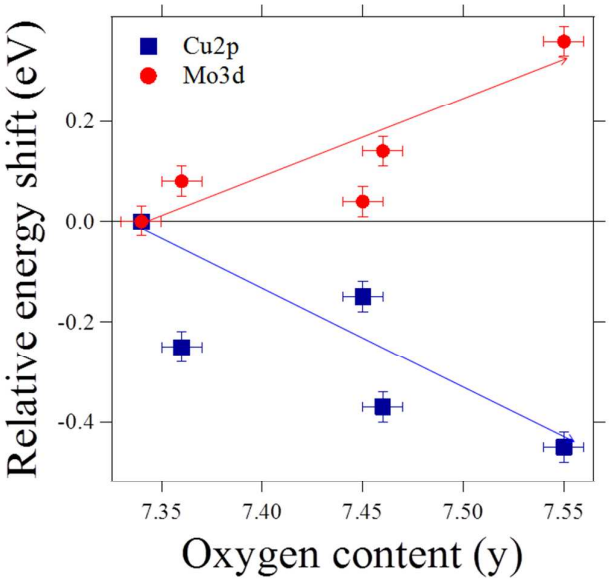

Figure 9. The relative energy shift of the Mo3d and Cu2p core level spectra with oxygenation in $Mo_{0.3}Cu_{0.7}Sr_2RECu_2O_y$. It emphasizes the shift of the Mo3d and Cu2p core level spectra in opposite sides of the energy region, pointing out the simultaneous oxidation of Mo and reduction of Cu.

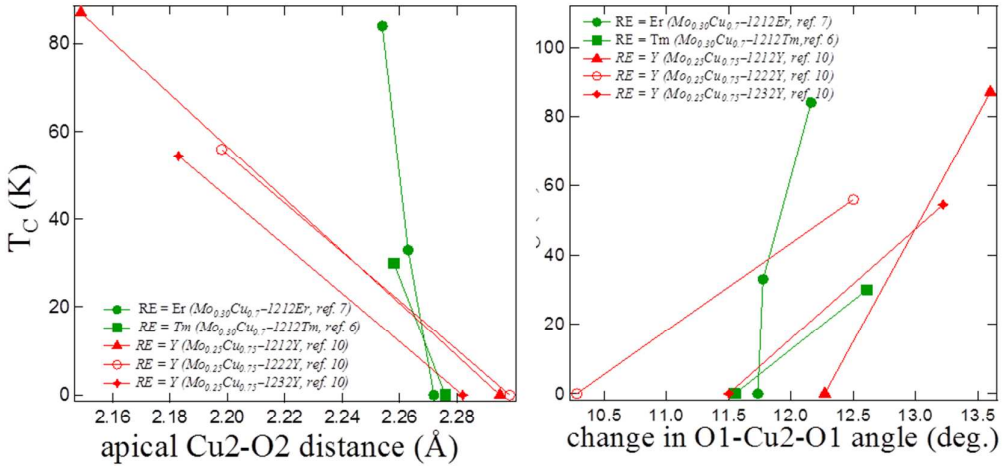

Figure10. Variation of the superconducting transition temperatures (T_C) with (a) the apical Cu2-O2 distances and (b) buckling angle (O1-Cu2-O1 angle) for different $Mo_xCu_{1-x}Sr_2RECu_2O_y$ (RE = Y, Er and Tm, ref. 10, 7 and 6) samples. It clearly shows that T_C increases in parallel with the shortening of the apical O distance (Cu2-O2) and increasing CuO_2 plane buckling, while the two orbital model[17,45] predicts the opposite effect (see text).

Tables:

Table 1. Sample annealing (oxygenation process) conditions, their naming details, superconducting transition temperatures (T_C), calculated oxygen contents, TEP values at 290 K and the calculated hole concentrations (P_h) for the different $Mo_{0.3}Cu_{0.7}Sr_2ErCu_2O_y$ samples.

Preparation conditions	Sample name	T_C (K)	Oxygen content (y)	S (290 K) in μV/K	P_h
1273 K for 48 h in air	AP	NON SC	7.34 (NPD)	117.5	0.035
AP sample annealed under O_2 flow at 873 K for 48 h	OA	32 K	7.45 (NPD)	29.6	0.092
OA sample annealed under O_2 flow at 673 K for 24 h	OA1	25 K	7.36 (TGA)	32.8	0.089
AP sample annealed at 673 K for 48 hour under high oxygen pressure (pressure = 100 bar)	OAHP	45 K	7.46 (TGA)	24.5	0.097
Oxygenation of the AP sample in a Belt Press type apparatus at 5 GPa and 773 K for 30 min in the presence of 33 mol % $KClO_3$	HPO	84 K	7.55 (NPD)	–	–
Oxygenation of the AP sample in a Belt Press type apparatus at 8 GPa and 773 K for 30 min in the presence of 33mol% $KClO_3$	HPO_80kbar	89 K	7.58 (TGA)	–	–

Table 2. Parameters and summary of fitting of the Sr 3d XPS core level spectra for $Mo_{0.3}Cu_{0.7}Sr_2ErCu_2O_y$ samples.

Sample Name	Core-level spectra	B. E (eV)	FWHM	I (LBE)/I (HBE)
AP	(LBE) Sr $3d_{5/2}$	132.3	1.4	1.00/0.54
	$3d_{3/2}$	134.1		
	(HBE) Sr $3d_{5/2}$	133.4	1.6	
	$3d_{3/2}$	135.2		
OA	(LBE) Sr $3d_{5/2}$	132.2	1.5	1.00/0.50
	$3d_{3/2}$	134.0		
	(HBE) Sr $3d_{5/2}$	133.4	1.6	
	$3d_{3/2}$	135.2		
OA1	(LBE) Sr $3d_{5/2}$	132.0	1.5	0.99/1.00
	$3d_{3/2}$	133.8		
	(HBE) Sr $3d_{5/2}$	133.3	1.6	
	$3d_{3/2}$	135.1		
OAHP	(LBE) Sr $3d_{5/2}$	132.0	1.4	0.99/1.00
	$3d_{3/2}$	133.8		
	(HBE) Sr $3d_{5/2}$	133.3	1.5	
	$3d_{3/2}$	135.1		
HPO	(LBE) Sr $3d_{5/2}$	132.4	1.5	0.91/1.00
	$3d_{3/2}$	134.2		
	(HBE) Sr $3d_{5/2}$	133.5	1.5	
	$3d_{3/2}$	135.3		

Table 3. Parameters and summary of fitting of the Mo 3d XPS core level spectra for $Mo_{0.3}Cu_{0.7}Sr_2ErCu_2O_y$ samples.

Sample Name with T_C in K	Core-level spectra	B. E (eV)	Mo^V/Mo^{VI}	Average oxidation state	y
AP (0 K)	Mo^V $3d_{5/2}$	232.0	0.76/0.24	5.24	7.34
	$3d_{3/2}$	235.1			
	Mo^{VI} $3d_{5/2}$	232.9			
	$3d_{3/2}$	236.0			
OA (32 K)	Mo^V $3d_{5/2}$	231.9	0.71/0.29	5.29	7.45
	$3d_{3/2}$	235.0			
	Mo^{VI} $3d_{5/2}$	233.0			
	$3d_{3/2}$	236.1			

OA1 (25 K)	Mo^{V} $3d_{5/2}$ $3d_{3/2}$ Mo^{VI} $3d_{5/2}$ $3d_{3/2}$	232.0 235.1 233.1 236.2	0.70/0.30	5.30	7.36
OAHP (45K)	Mo^{V} $3d_{5/2}$ $3d_{3/2}$ Mo^{VI} $3d_{5/2}$ $3d_{3/2}$	231.9 235.0 233.0 236.1	0.69/0.31	5.31	7.46
HPO (84 K)	Mo^{V} $3d_{5/2}$ $3d_{3/2}$ Mo^{VI} $3d_{5/2}$ $3d_{3/2}$	231.9 235.0 233.0 236.1	0.60/0.40	5.40	7.55

Table 4. Parameters and summary of fitting of the Cu 2p XPS core level spectra for $Mo_{0.3}Cu_{0.7}Sr_2ErCu_2O_y$ samples.

Sample Name with T_C in K	Core-level spectra	B. E (eV)	FWHM	Cu^{II}:Cu^{III}	I_S/I_M	y
AP (0 K)	Cu^{II} $2p_{3/2}$ Cu^{III} $2p_{3/2}$	933.1 934.8	2.00 2.00	0.80:0.20	0.26	7.34
OA (32 K)	Cu^{II} $2p_{3/2}$ Cu^{III} $2p_{3/2}$	933.2 935.2	2.17 2.17	0.85:0.15	0.19	7.45
OA1 (25 K)	Cu^{II} $2p_{3/2}$ Cu^{III} $2p_{3/2}$	933.1 935.0	2.00 2.00	0.84:0.16	0.16	7.36
OAHP (45K)	Cu^{II} $2p_{3/2}$ Cu^{III} $2p_{3/2}$	933.0 934.8	2.02 2.02	0.88:0.12	0.16	7.46
HPO (84 K)	Cu^{II} $2p_{3/2}$ $Cu^{III}2p_{3/2}$	933.1 934.7	1.92 2.13	0.91:0.09	0.12	7.55